The stoichiometry of scaffold complexes in living neurons -DLC2 functions as a dimerization engine for GKAP

Enora Moutin, Vincent Compan, F. Raynaud, Caroline Clerte, Nathalie Bouquier, Gilles Labesse, Matthew L Ferguson, Laurent Fagni, Catherine A Royer, Julie Perroy

The stoichiometry of scaffold complexes in living neurons – DLC2 functions as a dimerization engine for GKAP

Enora Moutin[1,2,3], Vincent Compan[4], Fabrice Raynaud[1,2,3], Caroline Clerté[5,6], Nathalie Bouquier[1,2,3], Gilles Labesse[5,6], Matthew L. Ferguson[5,6], Laurent Fagni[1,2,3], Catherine A. Royer[5,6,*,‡] and Julie Perroy[1,2,3,‡]

ABSTRACT

Quantitative spatio-temporal characterization of protein interactions in living cells remains a major challenge facing modern biology. We have investigated in living neurons the spatial dependence of the stoichiometry of interactions between two core proteins of the N-methyl-D-aspartate (NMDA)-receptor-associated scaffolding complex, GKAP (also known as DLGAP1) and DLC2 (also known as DYNLL2), using a novel variation of fluorescence fluctuation microscopy called two-photon scanning number and brightness (sN&B). We found that dimerization of DLC2 was required for its interaction with GKAP, which, in turn, potentiated GKAP self-association. In the dendritic shaft, the DLC2–GKAP hetero-oligomeric complexes were composed mainly of two DLC2 and two GKAP monomers, whereas, in spines, the hetero-complexes were much larger, with an average of ~16 DLC2 and ~13 GKAP monomers. Disruption of the GKAP–DLC2 interaction strongly destabilized the oligomers, decreasing the spine-preferential localization of GKAP and inhibiting NMDA receptor activity. Hence, DLC2 serves a hub function in the control of glutamatergic transmission by ordering GKAP-containing complexes in dendritic spines. Beyond illuminating the role of DLC2–GKAP interactions in glutamatergic signaling, these data underscore the power of the sN&B approach for quantitative spatio-temporal imaging of other important protein complexes.

KEY WORDS: Bioluminescence resonance energy transfer, Dynein light chain, Guanylate kinase-associated protein, Oligomerization, Scaffold, Scanning number and brightness

INTRODUCTION

At brain excitatory synapses, changes in synaptic strength underlie molecular memory and learning-related synaptic plasticity. To allow both for long-term maintenance of synaptic transmission and acute changes in synaptic strength, the function of individual receptors must be tightly regulated. Although normally devoid of catalytic activity, scaffold proteins have a significant impact on controlling the flow of signaling information. By assembling receptors with signaling proteins into complexes, often referred to as receptosomes, scaffolds play the part of signal-processing hubs (Zeke et al., 2009). These protein–protein interactions within a receptosome are highly dynamic and are involved in regulating synaptic receptor density and function in space and time (Renner et al., 2008). Protein oligomerization provides new opportunities for functional control, such as allosteric regulation and the establishment of higher-order complexity. Multiple functions for a given scaffold might arise from the composition and stoichiometry of the scaffold complex. Importantly, defects in scaffold expression or impairments in protein–protein interactions might underlie various neurological disorders (Bockaert et al., 2010). Hence, deciphering the precise organization and stoichiometry of scaffolds in specific sub-cellular compartments in living neurons might help to define new therapeutic targets for discrete modulation of functional oligomerization relevant to a given pathology.

Despite the urgent need for such information, the quantitative characterization of protein interactions in live cells remains one of the most difficult challenges in modern biology. Here, we used an innovative approach in fluorescence fluctuation microscopy, scanning number and brightness (sN&B) in two-photon mode (Digman et al., 2009), to spatially quantify the existence and stoichiometry of proteins complexes in various subcellular compartments in living neurons. This approach uses the second moment (variance) of the fluorescence intensity distribution of fluorescently labeled proteins at all pixels from multiple rapid raster scans to deconvolve the fluorescence signal into the number of particles (concentration) and their individual molecular brightness (stoichiometry). In two-color mode, the covariance of the fluorescence intensities in two channels allows the calculation of the cross-brightness, a direct measure of interaction between two fluorescently labeled protein fusions of different colors.

One major mechanism to induce persistent changes in synaptic strength involves the activation of N-methyl-D-aspartate (NMDA) receptors at the synaptic plasma membrane. The synaptic localization, clustering and function of NMDA receptors are controlled by their capacity to interact with scaffolds. As a core protein of the scaffolding complex, the guanylate-kinase-associated protein (GKAP, also known as DLGAP1) physically links glutamate NMDA receptors to type I metabotropic glutamate receptors through the PSD-95–GKAP–Shank–Homer scaffold complex (Naisbitt et al., 1999; Scannevin and Huganir, 2000; Tu et al., 1999). GKAP also interacts with the dynein light chain [DLC, also known as LC8 and DYNLL (Naisbitt et al., 2000)]. DLC is an essential component of the dynein and myosin V molecular motors (Benashski et al., 1997), but is also found in numerous other complexes (Fejtova et al., 2009; Fuhrmann et al., 2002; Jaffrey and Snyder, 1996; Lo et al., 2005; Puthalakath et al., 1999; Raux et al., 2000; Schnorrer et al., 2000). Thus, in addition to

[1]CNRS, UMR-5203, Institut de Génomique Fonctionnelle, Montpellier, F-34094, France. [2]INSERM, U661, Montpellier, F-34094, France. [3]Universités de Montpellier 1 & 2, UMR-5203, Montpellier, F-34094, France. [4]Faculty of Life Sciences, University of Manchester, Manchester M13 9PT, UK. [5]Centre de Biochimie Structurale, INSERM U1054, Montpellier, F-34090, France. [6]CNRS UMR5048, Universités Montpellier 1 and 2, Montpellier F-34090, France.
*Present address: Departments of Biological Sciences and Chemistry, Rensselaer Polytechnic Institute, Troy, NY 12180 USA.

‡Authors for correspondence (royerc@rpi.edu; julie.perroy@igf.cnrs.fr)

its role in transport as a molecular motor light chain (Lee et al., 2006; Navarro et al., 2004; Schnorrer et al., 2000), DLC could be an ordered hub protein as well, promoting the oligomerization and ordering of the natively disordered monomeric proteins with which it interacts (Benison et al., 2006; Nyarko et al., 2004; Wang et al., 2004). In this work, we investigated the role of the GKAP–DLC2 interaction in scaffold organization, which impacts on the regulation of NMDA receptor function in synaptic transmission.

We found that dimerization of DLC2 is required for its binding to GKAP. Dimeric DLC2 then functions to promote the self-association of GKAP in dendritic spines. Combining sN&B with electrophysiological recordings, we underscore the function of this oligomeric complex in the potentiation of glutamate receptor activity. Hence, the present study highlights the hub function of DLC2 in the brain, where it binds to partially disordered GKAP proteins to promote their structural organization and oligomerization, thereby sustaining adequate glutamate receptor signaling and accurate synaptic transmission.

RESULTS

Dimeric DLC2 interacts with GKAP to potentiate GKAP self-association

DLC is thought to be predominantly dimeric under physiological conditions (Benashski et al., 1997). This dimerization is presumed to be a prerequisite for its interaction with its partners (Rapali et al., 2011), because the monomer lacks the partner-protein-interaction groove (Makokha et al., 2004; Wang et al., 2003). Co-immunoprecipitation of mCherry–DLC2 and Venus–DLC2 confirmed the homo-oligomerization of DLC2 in human embryonic kidney (HEK) cells (Fig. 1A). Interestingly, electrostatic interactions at the dimer interface are thought to contribute to the DLC monomer-dimer equilibrium (Benison et al., 2009). Notably, DLC1 dimerization is disrupted by phosphorylation at a specific Ser88 residue at the interface, resulting in the formation of an inactive monomer (Song et al., 2008; Song et al., 2007; Xiao et al., 2010). We engineered point mutations on DLC2 to mimic the phosphorylated form (DLC2-S88E) or to prevent phosphorylation of DLC2 (DLC2-S88A). The mutant lacking the phosphorylation site displayed an ability to oligomerize similar to that of the wild-type protein, as shown by the co-immunoprecipitation of Venus–DLC2-S88A with mCherry–DLC2 ($-2.1\pm13.7\%$ compared with wild-type Venus–DLC2; $\pm$s.e.m.). By contrast, mimicking constitutive phosphorylation on Ser88 (Venus–DLC2-S88E) strongly impaired its dimerization with mCherry–DLC2 ($-84.5\pm5.6\%$ compared with Venus–DLC2, Fig. 1A), providing an efficient tool to compare the interaction of the obligate-monomeric DLC2 mutant versus that of oligomeric DLC2 with GKAP. Co-immunoprecipitation of Cerulean–GKAP with mCherry–DLC2 (Fig. 1B) confirmed previous results showing that GKAP interacts with DLC2 (Moutin et al., 2012a; Naisbitt et al., 2000). By contrast, GKAP failed to immunoprecipitate with the obligate monomeric DLC2-S88E mutant (Fig. 1B). We next assessed GKAP–DLC2 interactions in living cells by using bioluminescence resonance energy transfer (BRET), with *Renilla* luciferase (Rluc8)–GKAP and Venus–DLC2 constructs (Moutin et al., 2012a). Under conditions of constant Rluc8–GKAP expression, the BRET signal increased hyperbolically as a function of the Venus–DLC2 expression level (Fig. 1C), indicating an effective interaction between GKAP and DLC2 in living cells. By contrast, coexpression of Rluc8–GKAP and Venus–DLC2-S88E led to weaker signals that increased linearly rather than hyperbolically with the increase in the fluorescence:luminescence ratio, most likely reflecting random collision (bystander BRET) between GKAP and the obligate-monomeric DLC2 mutant (Fig. 1C). Taken together, these results highlight the interaction between GKAP and DLC2 but not DLC2-S88E, suggesting that GKAP interacts exclusively with the dimeric DLC2.

We investigated next whether GKAP could self-associate in its intact cellular environment using BRET. The N-terminus of GKAP was fused to the energy donor RLuc8 or to the acceptor entity Venus (RLuc8–GKAP and Venus–GKAP). Addition of the tag does not impair the expression of GKAP in dendritic spines of cultured hippocampal neurons nor its interaction with PSD-95 (also known as DLG4) and Shank3 (Moutin et al., 2012a). Under conditions of constant RLuc8–GKAP expression levels, the BRET signal increased hyperbolically as a function of Venus–GKAP expression level (Fig. 2A), indicating an effective interaction between GKAP proteins in living cells. The ratio 'fluo:lumi$_{50}$' of acceptor:donor molecules yielding 50% of the maximal energy transfer (BRET$_{50}$) is a reflection of the relative apparent affinity of the acceptor fusion for the donor fusion proteins (Mercier et al., 2002). We found that RLuc8–GKAP and Venus–GKAP interacted with an apparent relative affinity of fluo:lumi$_{50}$ of $19.6\pm3.3\times10^{-3}$ ($\pm$s.e.m.). A GKAP mutant that cannot interact with DLC2 (Rluc8–GKAPmut) – because the molecular regions involved in the interaction with DLC2 are mutated (Moutin et al., 2012a) – displayed similar apparent relative affinity for itself (fluo:lumi$_{50}$ $=28.7\pm6.0\times10^{-3}$), demonstrating that GKAP dimerization in living cells does not require DLC2 (Fig. 2A). However, co-transfection of DLC2 significantly increased the ability of GKAP (but not GKAPmut) to self-associate (in the presence of DLC2, fluo:lumi$_{50}=3.3\pm0.5\times10^{-3}$ for GKAP and $22.3\pm2.6\times10^{-3}$ for GKAPmut, Fig. 2A). Thus, even though DLC2 was not absolutely required, the apparent affinity of GKAP self-association was sevenfold higher in the presence of DLC2, suggesting that GKAP self-association is potentiated by its interaction with DLC2.

To further characterize the oligomeric state of GKAP and the potential role of DLC2, we performed cross-linking experiments in living HEK cells. We found that $22.2\pm5.0\%$ of GKAP was assembled as homo-oligomers, whereas the remainder was monomeric (Fig. 2B). Interestingly, the mutant of GKAP (GKAPmut) that cannot interact with DLC2 displayed a similar self-association ability to that of the wild-type GKAP ($26.6\pm3.9\%$ of proteins assembled as dimers, Fig. 2B), confirming that DLC2 is not required for the GKAP–GKAP interaction. Nonetheless, co-transfection of DLC2 with wild-type GKAP induced a significant increase in GKAP oligomerization ($+37.8\pm9.4\%$ of GKAP assembled as homodimers, Fig. 2C), indicating a strong DLC2-mediated potentiation of GKAP self-association. Furthermore, DLC2-S88A, which forms homodimers (Fig. 2C, anti-RFP), also increased the GKAP oligomer:monomer ratio by $30.7\pm15.6\%$ (Fig. 2C, anti-GFP). By contrast, DLC2-S88E, which is an obligate monomer (Fig. 2C, anti-RFP), did not affect GKAP dimerization ($-11.4\pm6.6\%$ compared with GKAP alone, Fig. 2C), consistent with the absolute requirement of DLC2 dimerization for its interaction with GKAP (Fig. 1) and subsequent promotion of GKAP self-association. These results demonstrate that GKAP self-associates and that, although not strictly necessary, dimers of DLC2 interacting with GKAP strongly favor this self-association.

Structural modeling of the DLC2–GKAP complexes: DLC2 dimer binding of two GKAP monomers would enable high-order species

Based on GKAP sequences and the known DLC2 crystal structure, we predicted aspects of the three-dimensional

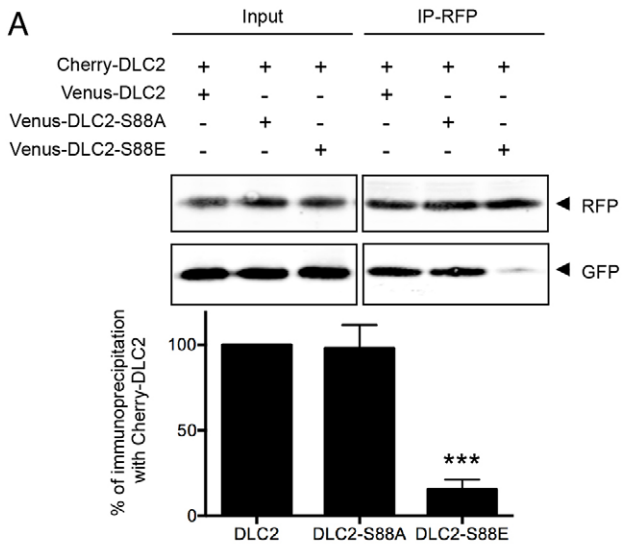

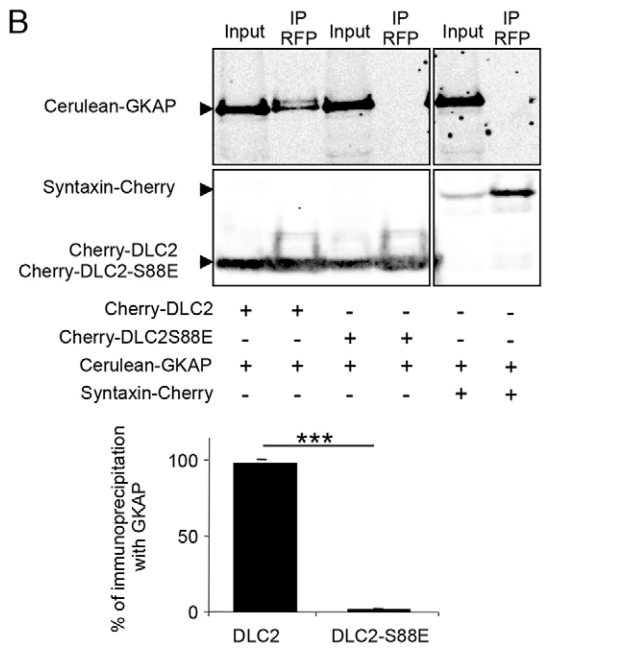

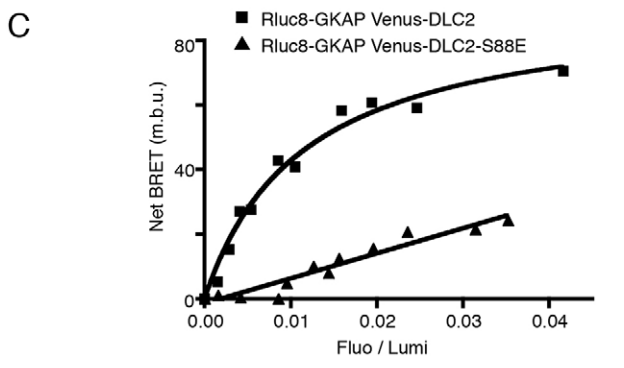

Fig. 1. Unphosphorylated DLC2 forms oligomers, which interact with GKAP. (A) HEK293 cells were co-transfected with mCherry–DLC2 and Venus–DLC2, Venus–DLC2-S88A or Venus–DLC2-S88E expression plasmids. mCherry–DLC2 and Venus–DLC2, Venus–DLC2-S88A or Venus–DLC2-S88E proteins were detected by immunoblotting before (Input) and after (IP-RFP) immunoprecipitation of mCherry–DLC2 with RFP–Trap, using the anti-RFP and anti-GFP antibodies to detect mCherry–DLC2 and Venus-tagged proteins, respectively. To quantify the immunoprecipitations (IP-RFP), the ratios of Venus–DLC2-S88A:mCherry–DLC2 and Venus–DLC2-S88E:mCherry–DLC2 were expressed as a percentage of the ratio of Venus–DLC2:mCherry–DLC2. Data show the mean±s.e.m. (three individual experiments); ***$P<0.0001$ (Mann-Whitney *U*-test). (B) HEK293 cells were co-transfected with Cerulean–GKAP and mCherry–DLC2 or mCherry–DLC2-S88E expression plasmids. mCherry–DLC2 or mCherry–DLC2-S88E were immunoprecipitated with RFP-Trap, and the amount of Cerulean–GKAP that co-immunoprecipitated was quantified by western blotting analysis using the anti-GFP antibody. The control assay was performed under the same conditions but with syntaxin–mCherry instead of mCherry–DLC2 or mCherry–DLC2-S88E (last lane). For the immunoprecipitations, the ratio of Cerulean–GKAP:mCherry–DLC2-S88E was expressed as a percentage of the ratio of Cerulean–GKAP:mCherry–DLC2. Data show the mean±s.e.m. (three individual experiments); ***$P<0.0001$ (Mann-Whitney *U*-test). (C) HEK293 cells were co-transfected with constant concentrations of RLuc8–GKAP and increasing concentrations of Venus–DLC2 or Venus–DLC2-S88E expression plasmids. BRET was expressed as a function of the Venus–DLC2 or Venus–DLC2-S88E acceptor expression levels. Individual readings obtained from three independent experiments were pooled. Curves were fitted using a nonlinear regression equation (GraphPadPrism), assuming a single binding site.

structure of their complex. The three-dimensional structure of GKAP has not been determined to date. Little or no stable secondary structure is predicted for the first half of the sequence, whereas four long helices are predicted in the second half, preceding the C-terminal PDZ-binding motif. These predicted coiled-coils could correspond to a dimerization site for GKAP–GKAP interactions. Roughly 100 residues prior to the first coiled-coil, two β-strands are predicted (Cole et al., 2008). These two predicted strands correspond to two motifs conserved among the GKAP homologs, the consensus sequences of which (339-SIGIQVD-345 and 364-SVGVQVE-370, respectively) match the recognition motif for DLC2 binding (Fig. 3A). We analyzed the possible interaction of the conserved motifs with DLC2, taking advantage of the high-resolution crystal structure of DLC2 in complex with 'optimized' peptides (Rapali et al., 2011). Although the consensus sequence of the optimized peptide (SRGTQTE) appears dissimilar from the conserved segments in GKAP, the structural analysis revealed, first, the importance of the conserved residues S, G and Q at positions 1, 3 and 5, but also that the substitutions T to V or I are acceptable at positions 4 and 6. Indeed, the few hydrogen bonds lost with these substitutions are predicted to be compensated for by the favorable van der Waals contacts with surrounding hydrophobic residues lining the binding pocket in DLC2 (e.g. Tyr75 and Leu84 for the recognition of V or I at the fourth position). Similarly, a hydrophobic valine or isoleucine at position 2 can be accommodated thanks to the hydrophobic environment (Phe73). In parallel, the branched residues valine and isoleucine are highly favorable for the extended conformation observed in the bound peptide, and they will promote binding through favorable desolvation of their hydrophobic sidechains. Furthermore, similar substitutions were observed in the peptides recognized by the highly similar DLC1 (Liang et al., 1999), the binding groove of which is perfectly conserved compared with that of DLC2.

According to this structural survey, the two conserved motifs can be recognized by DLC2, suggesting two possible models: either one dimer of DLC2 can bind to one GKAP by interacting with its two motifs (Fig. 3B) or, alternatively, one DLC2 dimer binds to two distinct GKAP molecules (Fig. 3C). The side-by-side dimerization of DLC2 implies that each peptide must run in

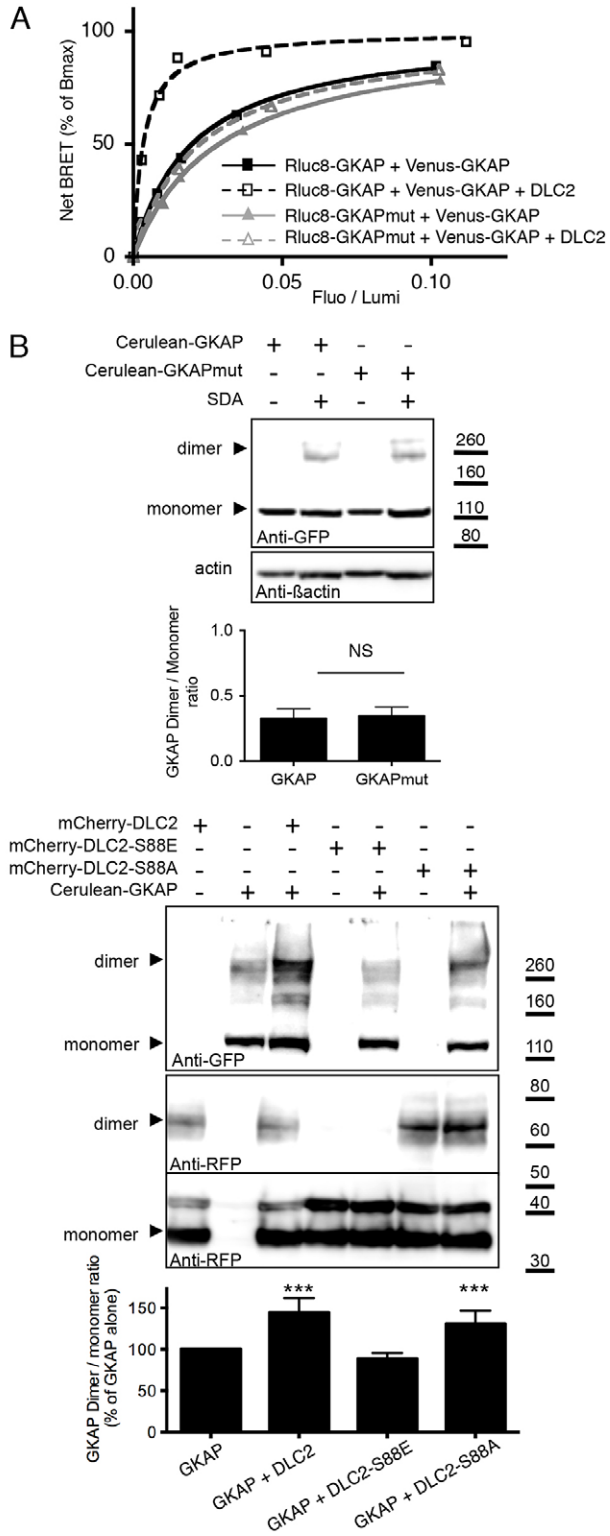

Fig. 2. GKAP forms dimers, which are favored by the interaction with DLC2. (A) HEK293 cells were co-transfected with constant concentrations of RLuc8–GKAP or Rluc8–GKAPmut and increasing concentrations of Venus–GKAP, with or without DLC2 expression plasmids. BRET was expressed as a function of the Venus–GKAP acceptor expression level. Individual readings obtained from three independent experiments were pooled. The curve was fitted using a nonlinear regression equation (GraphPadPrism), assuming a single binding site. (B) HEK293 cells transfected with the indicated expression plasmids were treated with NHS-LC-Diazirine (SDA), to cross-link the oligomers, or left untreated. The dimer:monomer ratio of Cerulean–GKAP and Cerulean–GKAPmut proteins were quantified by western blot analysis using the anti-GFP antibody. Actin staining was used to control protein loading. (C) Cells were transfected as in B, and all conditions were cross-linked with SDA. mCherry–DLC2 expression was assessed by using the anti-RFP antibody. The dimer:monomer ratio of Cerulean–GKAP in each condition was expressed as a percentage of the ratio obtained with Cerulean–GKAP alone. Data show the mean±s.e.m. (three individual experiments); ***$P<0.0001$; NS, non-significant (Mann-Whitney *U*-test).

the same direction in each binding groove. The shortest distance between the N-terminus of one bound peptide and the C-terminus of the second bound peptide (~2.8 nm running through the DLC2 dimer core and >4.5 nm if the GKAP peptide tightly wraps a DLC2 dimer) is incompatible with the sequence length separating the two conserved motifs in GKAP (15 to 20 residues, depending on the species considered). Furthermore, the highly variable and hydrophilic nature of the residues in this joining segment argues against a strong interaction with the DLC2 core, in contradiction with the 2:1 DLC2:GKAP model (shown in Fig. 3B). These considerations of distance and the volume of a DLC2 monomer provide the basis for an argument against the occupation of both sites on the DLC2 dimer by a single GKAP monomer. Accordingly, a more probable 2:2 model is that of a DLC2 dimer binding to two GKAP monomers (Fig. 3C), which could themselves recruit other DLC2 molecules thanks to their second motif, making possible the formation of higher-order species.

The amount of and association between GKAP and DLC2 varies among sub-cellular compartments in neurons

To characterize the organization of GKAP and DLC2 in the scaffolding complex in different subcellular neuronal compartments, we used a novel variation of fluorescence fluctuation microscopy, sN&B, in two-photon mode (Digman et al., 2008). This approach measures fluctuations in fluorescence intensity in a small two-photon excitation volume (~0.3 fl). Deconvolution of the average intensity, $\langle F \rangle$ (counts/s), into the molecular brightness B (counts/s/molecule)×N (number of molecules) using intensity fluctuations, as described in Materials and Methods, allows the assessment of the degree of homo-oligomerization of mCherry-tagged or Cerulean-tagged proteins. The covariance between the intensity fluctuations (Bcc) in two detection channels (red channel for the detection of mCherry; blue channel for the detection of Cerulean) allows evaluation of the degree of hetero-oligomerization (Digman et al., 2009). A non-zero value of Bcc indicates the formation of hetero-complexes. For fluorescence intensity fluctuations to be observed in the two-photon point spread function (PSF) (ω_o=400 nm, z_o=1.4 μm) at each pixel in a series of frames, the pixel sampling or dwell time (50 μs in this case) must be faster than diffusion (for free GFP in cells, diffusion is on the ms timescale, 20-fold slower than the sampling time), so as to avoid averaging. By contrast, the frame time (~4 s in this study) must be slower than the diffusion of the protein complexes, in which case fluctuations due to molecular diffusion are detected for a given pixel in successive frames. Any motion slower than the 50-μs dwell time and faster than the 4-s frame time will lead to fluctuations in fluorescence due to particles moving in and out of the PSF. Here, we have chosen to use GKAP and DLC2 fused to the fluorescent proteins Cerulean and mCherry, respectively. We used an excitation wavelength of 930 nm, on the red edge of the Cerulean two-photon cross section and on the blue edge of that

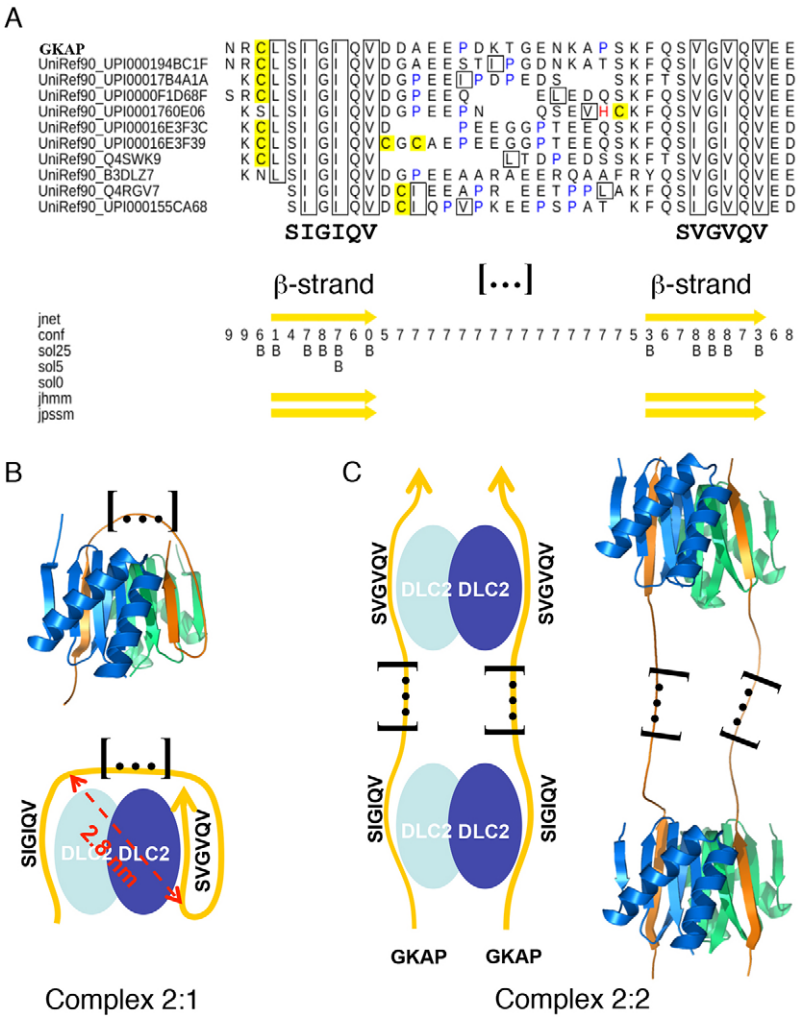

Fig. 3. Predicted models for molecular scaffold organization. (A) Sequence alignment and secondary structure predictions by the server Jpred3 are shown for the region containing the two consensus sequences of GKAP (S#G#Q#, where the symbol '#' stands for any hydrophobic residue) that match the DLC2 recognition motif (SxGxQx). Predicted β-strands are highlighted by yellow arrows, and square brackets (in A–C) indicate the recurrence of numerous deletions among close homologs. Color-coding is as generated by the JPRED server: boxed sequence, conserved hydrophobic residues forming the core of the two motifs; yellow highlighting, cysteines (disulfide bridges); blue text, prolines (kinks); red text, histidines (catalysis or metal binding). From the predicted local structure, two alternative models can be proposed, the complex 2:1 model (shown in B) and the complex 2:2 model (shown in C). (B) Upper panel, one dimer of DLC2 (blue and green ribbons) binds to one GKAP molecule (orange ribbon) by recognizing its two motifs. Lower panel, schematic representation of the ribbon diagram shown in the upper panel. (C) Right, two DLC2 dimers (green and blue ribbons) can bind to two distinct GKAP molecules (orange ribbon). Left, schematic representation of the ribbon diagram. Given the rather short and variable sequence length separating the two conserved motifs (~18±3 residues), the 2:1 model in which one GKAP molecule wraps around a DLC2 dimer to occupy the two binding sites is unlikely. The most likely hypothesis is that a dimer of DLC2 binds to two GKAP molecules (C), which could themselves bind to other molecules of DLC2 thanks to their second motif. The figure was drawn using Pymol.

for mCherry. This fluorescent protein pair does not undergo fluorescence resonance energy transfer (FRET), and Cerulean exhibits no bleedthrough into the mCherry channel in our optical system. Indeed, bleedthrough would give rise to artifactual positive cross-brightness, whereas FRET would actually be anti-correlated. The major advantage of two-photon sN&B cross-brightness measurements is that one obtains a diffraction-limited, spatially resolved quantitative image of the existence of protein complexes. Moreover, this cross-brightness measurement is shot-noise free, allowing for very high sensitivity detection of complexes. The individual brightness values in two-channel detection provide information concerning the stoichiometries of the complexes. Finally, two-photon excitation, coupled with the fast scanning, allows simultaneous excitation with one laser line of two spectrally distinct fluorescent proteins and greatly diminishes photobleaching problems, while, at the same time, yielding much lower autofluorescent background than is observed with visible lasers.

We transfected primary cultures of hippocampal neurons with mCherry–DLC2 and Cerulean–GKAP. The two proteins were detected in all cellular compartments of hippocampal neurons in culture (Fig. 4A, F1 and F2). Fluorescence intensity in channel 1 (F1) showed that mCherry–DLC2 was distributed throughout the dendritic shaft and spines (spine:shaft ratio for F1=1.12±0.08, Fig. 4A). In both shaft and spines, relatively high values of molecular brightness, B1, revealed the formation of DLC2–DLC2 homo-oligomers (Fig. 4A). Cerulean–GKAP (F2) was also expressed in the dendritic process but with a preferential expression in spines (spine:shaft ratio for F2=2.17±0.09, Fig. 4A). GKAP–GKAP homo-oligomeric complexes were found mostly in spines (note the high B2 values in spines in Fig. 4A). Interestingly, GKAP and DLC2 were also engaged in DLC2–GKAP hetero-interactions in the spines, whereas the hetero-oligomers were much less apparent in the shaft (Bcc, Fig. 4A). In some instances, we also found intracellular pools showing higher expression levels (F1 and F2, Fig. 4A), but a relatively low degree of interaction between the two proteins as compared with that observed in the spines (Bcc, Fig. 4A,C). Hence, these sN&B results suggested that DLC2, as well as GKAP, could form homo-complexes in neurons that could also interact with each other to a degree that depended on subcellular localization.

Impairment of the DLC2–GKAP interaction decreases GKAP–GKAP interaction in spines

To investigate the role of GKAP–DLC2 interactions in the organization and composition of the scaffold complex, we engineered peptides with a dominant-negative effect on the GKAP–DLC2 interaction based on the structural modeling above, assuming that the GKAP amino acid sequences GIQVD and

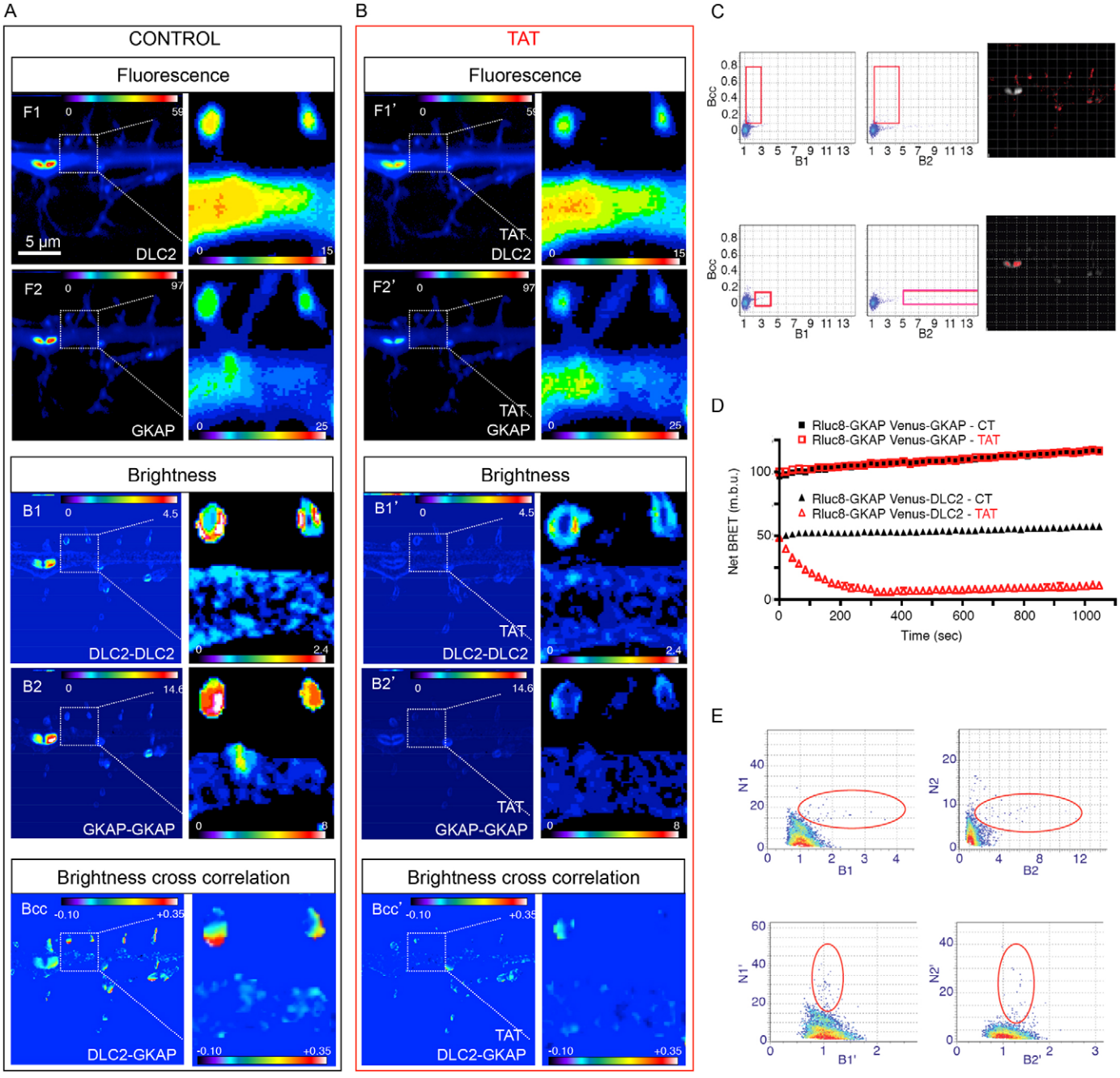

Fig. 4. GKAP and DLC2 are assembled into hetero-oligomers in dendritic spines. (A,B) sN&B was performed on hippocampal neurons transfected with mCherry–DLC2 and Cerulean–GKAP expression plasmids, before (A) and after (B) disruption of the GKAP–DLC2 interaction by TAT treatment. The boxed region of each image is shown at higher magnification to the right; sN&B was used to analyze the dendritic processes of hippocampal neurons transfected with mCherry–DLC2 and Cerulean–GKAP expression plasmids. The images show: (1) The fluorescence of mCherry–DLC2 and Cerulean–GKAP proteins before (F1 and F2, respectively) and after (F1′ and F2′) TAT treatment. The fluorescence indicates protein expression in subcellular neuronal compartments. (2) The brightness of mCherry–DLC2 and Cerulean–GKAP proteins before (B1 and B2, respectively) and after (B1′ and B2′) the addition of TAT. The brightness indicates that DLC2 (B1 and B1′) and GKAP (B2 and B2′) undergo homo-oligomerization. (3) The cross brightness of mCherry–DLC2 and Cerulean–GKAP proteins before (Bcc) and after (Bcc′) the addition of TAT. Bcc values of >0 indicate hetero-oligomerization between GKAP and DLC2. (C) Pixel histograms (left, middle) of Bcc values as a function of the brightnesses of mCherry–DLC2 (B1) or Cerulean–GKAP (B2) and maps (right) highlighting in red the subcellular location of pixels selected on the corresponding graphs (red rectangle). High Bcc values with low B1 and B2 values were specifically found in spines (upper panels), whereas low Bcc values with high B1 and B2 values corresponded to pixels located in the intracellular pool of the neuron (lower panels). Thus, in the spines, GKAP and DLC2 form complexes with each other with relatively low stoichiometry of both proteins, whereas, in the intracellular pools, the degree of heterologous interaction is lower and the degree of homo-oligomerization is higher. (D) Specificity of TAT dominant-negative peptides in disrupting the GKAP–DLC2 interaction. BRET signal was recorded over time in HEK cells transfected with Rluc8–GKAP and Venus–DLC2 or Venus–GKAP, with or without the addition of TAT at time 0. TAT selectively decreased the BRET between Rluc8–GKAP and Venus–DLC2, but not Rluc8–GKAP and Venus–GKAP. (E) Pixel histograms of the number of DLC2-containing molecules (N1) or GKAP-containing molecules (N2) expressed as a function of the molecular brightness (B1 and B2), before (upper panel) and after (lower panel) the addition of TAT. Note that the scales are different. Red circles highlight a subset of pixels with high stoichiometry (B1 and B2) and low numbers of molecules (N1 and N2) that were disrupted by TAT into many molecules (high N1′ and N2′) with low stoichiometry (B1′ and B2′).

GVQVEE are the molecular determinants involved in the interaction with DLC2. We fused these two amino acid sequences (GIQVD and GVQVEE plus N-terminal extensions that are also involved in the binding motif, see Materials and Methods) to the cell-membrane-transduction domain of the human immunodeficiency virus (HIV-1) TAT protein (hereafter referred to as TAT). TAT-conjugated peptides can cross the plasma membrane, thus allowing their efficient internalization (Dietz and Bähr, 2005). We first validated the effectiveness and specificity of these dominant-negative peptides in disrupting the GKAP–DLC2 interaction. In HEK cells transfected with Rluc8–GKAP and Venus–DLC2, the addition of TAT peptides indeed decreased the BRET signal in a time-dependent manner (Fig. 4D), validating the efficiency of the dominant-negative peptides in the disruption of the GKAP–DLC2 interaction. By contrast, perfusion of the TAT did not affect the BRET signals over time in HEK cells transfected with Rluc8–GKAP and Venus–GKAP. This result highlights the selectivity of these peptides to disrupt GKAP–DLC2 interactions, but not GKAP–GKAP interactions, when expressed separately (Fig. 4D). On the same neurons as above, we analyzed the cross brightness between the mCherry–DLC2 and the Cerulean–GKAP proteins at 5 min after TAT addition (Fig. 4B, Bcc′). Addition of TAT led to substantial dissociation of the DLC2–GKAP complexes in all subcellular compartments, including the spines (Fig. 4A,B, compare Bcc and Bcc′), with little or no change in the total fluorescence intensity (Fig. 4A,B, F1 versus F1′, F2 versus F2′). Hence, GKAP and DLC2 form reversible heterologous complexes in all cellular compartments.

Surprisingly, disruption of the DLC2–GKAP interaction by addition of the dominant-negative peptides dramatically affected the individual brightness values of GKAP and DLC2 (Fig. 4B, B2′ and B1′, respectively), indicating the disruption of GKAP–GKAP and DLC2–DLC2 homo-interactions. Given that the TAT peptide uniquely and specifically disturbed the GKAP–DLC2 hetero-interaction (but did not directly affect GKAP–GKAP interactions, Fig. 4D), these data indicate that the impairment of the homo-oligomerization of DLC2–DLC2 and GKAP–GKAP in neurons was a consequence of the disruption of GKAP–DLC2 hetero-interaction. sN&B histograms from both channels (Fig. 4E) revealed a subset of pixels with high stoichiometry (B1 and B2) and low number of particles (N1 and N2) in absence of TAT, that switch to values of high N′ and low B′ in presence of these peptides (Fig. 4E, red circles). This analysis confirmed that small numbers of large DLC2–DLC2 and GKAP–GKAP complexes dissociated into large numbers of small complexes when TAT disrupts the GKAP–DLC2 interaction. These sN&B results confirmed our biochemical experiments showing that dimeric DLC2 interacts with GKAP to potentiate GKAP self-association (Figs 1, 2) and also suggested a reciprocal stabilization of the DLC2 homodimer by the interacting partners, promoting higher order hetero-oligomeric complexes.

Subcellular stoichiometry of GKAP and DLC2 complexes in neurons

To quantify in greater detail the stoichiometry of these complexes in the dendritic shaft versus dendritic spines, we took advantage of the TAT peptide. The true shot-noise-corrected brightness values of mCherry–DLC2 and Cerulean–GKAP ($\varepsilon = B - 1$) were calculated for the lowest intensity pixels in the dendritic shaft in presence of the TAT peptide. The average values were found to be $\varepsilon 1 = 0.033$ counts per 50-μs dwell-time per molecule (cpdpm) for mCherry–DLC2 and $\varepsilon 2 = 0.010$ cpdpm for Cerulean–GKAP. These very low values are consistent with particles containing only one fluorescent protein. We have indeed measured similar true brightness values in cells transfected with a plasmid bearing a nuclear localization sequence (NLS) sequence flanked by Cerulean on the N-terminus and mCherry on the C-terminus ($\varepsilon 1 = 0.026$ for mCherry and $\varepsilon 2 = 0.015$ for Cerulean) under similar imaging conditions. Assuming then that the values of the true brightness measured after disruption of the complex in the shaft regions correspond to monomers of each protein, we calculated the apparent stoichiometry of the GKAP and DLC2 oligomers prior to disruption by the TAT peptide (see Table 1 for ε1, ε2 and Bcc values).

In the dendritic shaft, the mean true brightness found prior to TAT addition for mCherry–DLC2 and Cerulean–GKAP corresponded to an average apparent stoichiometry of 2.4 and 2.0, respectively, with a Bcc of 0.013. We note that these stoichiometries are average and apparent values, arising from a linear weighted sum of mixtures of all oligomeric forms of the proteins in the selected pixels (monomers, dimers and tetramers, etc., which might or might not all participate in hetero-complexes). Nonetheless, these values are suggestive of a predominance of heterotetramers (a dimer of heterodimers) in this region.

We focused on dendritic spines to better comprehend the organization of proteins within complexes in this subcellular compartment, which is of particular functional interest. We found that, prior to the addition of the TAT peptide, the oligomers of DLC2 (B1) and GKAP (B2) were of higher order in spines compared with those in the shaft. The average true brightness values for the pixels in the spines yielded apparent average stoichiometries between ~16.5 and ~13.0 for both proteins (Table 1). This higher apparent stoichiometry for the two proteins in the spines compared with that observed in the shaft correlates with a higher degree of hetero-oligomerization (Bcc was 0.077 in spines compared with 0.013 in the shaft). Pixels in the spines exhibiting higher average Bcc also exhibited higher

Table 1. Mean apparent stoichiometry of DLC2–GKAP complexes

Transfection condition	Cellular region	<B1> (cpdpm)	<ε1> (cpdpm)	<B2> (cpdpm)	<ε2> (cpdpm)	Stoichiometry DLC2	Stoichiometry GKAP	<Bcc>
DLC2/GKAP	Shaft	1.075	0.075	1.018	0.018	2.4	2.0	0.013
	Spines	1.514	0.514	1.117	0.117	16.5	13.0	0.077
DLC2/GKAP+TAT	Shaft	1.033	0.033	1.010	0.010	1.1	1.1	0.009
	Spines	1.097	0.097	1.060	0.060	3.1	6.6	0.021
DLC2-S88E	Shaft	1.031	0.031	1.009	0.009	1.0	1.0	0.009
GKAP	Spines	1.087	0.087	1.055	0.055	2.8	6.1	0.047
DLC2	Shaft	1.040	0.040	1.011	0.011	1.3	1.2	0.008
GKAPmut	Spines	1.162	0.162	1.048	0.048	5.2	5.3	0.043

stoichiometries. Interestingly, disruption of the DLC2–GKAP interaction in the spines by the addition of TAT peptide affected the brightness of GKAP (B2′) and that of DLC2 (B1′) (Fig. 4A,B), indicating the suppression of complexes containing multimers of GKAP and multimers of DLC2 in dendritic spines. Indeed, the apparent average stoichiometry for the GKAP–GKAP complexes in spines decreased from ~13 to ~6 when DLC2–GKAP interactions were disrupted upon TAT addition, whereas that of DLC2–DLC2 decreased from ~16 to ~3. We confirmed these results by studying mutants with impaired ability to form hetero-interactions – mCherry–DLC2-S88E+Cerulean–GKAP or mCherry–DLC2+Cerulean–GKAPmut. It is noteworthy that, in both cases, the impairment in hetero-interaction (Bcc) was correlated with a strong decrease in DLC2 (B1) and GKAP (B2) stoichiometry (Table 1).

Disrupting GKAP–DLC2 oligomeric complexes decreases the preferential localization of GKAP in the spine and results in reduced NMDA currents

Given that the true number of molecules (*n*, see Materials and Methods) is measured in a focal volume of 0.3 μm^3, the average number of particles in a spine of 1 μm^3 was calculated to be ~159.0±5.1 (±s.e.m.) particles containing DLC2 and 66.1±2.2 particles containing GKAP. Moreover, analysis of the fluorescence intensities of DLC2 (F1′) and GKAP (F2′) in dendritic processes upon disruption of the GKAP–DLC2 interaction by the competitive TAT peptides revealed a significant relocalization of GKAP into the shaft (Fig. 4A,B, spine:shaft ratio=2.17±0.09 for F2 and 1.87±0.08 for F2′), whereas the broad localization of DLC2 was not significantly affected (Fig. 4A,B, spine:shaft ratio=1.12±0.08 for F1 and 1.17±0.10 for F1′). Disrupting the GKAP–DLC2 interaction thus decreased the preferential localization of GKAP in the spines.

Further insight into the role of GKAP–DLC2 oligomerization in synaptic transmission was obtained in functional analyses performed in the presence of TAT, which disrupts GKAP–DLC2 oligomers. We recorded endogenous NMDA currents in hippocampal neurons in the patch-clamp whole-cell configuration, before and during perfusion with TAT peptides. Interestingly, after 10 min of TAT peptide perfusion, NMDA currents were decreased by 47.3±4.3% (Fig. 5). These data show that the disruption of endogenous GKAP–DLC2 oligomers, which impairs GKAP dimerization, induces a strong inhibition of NMDA currents.

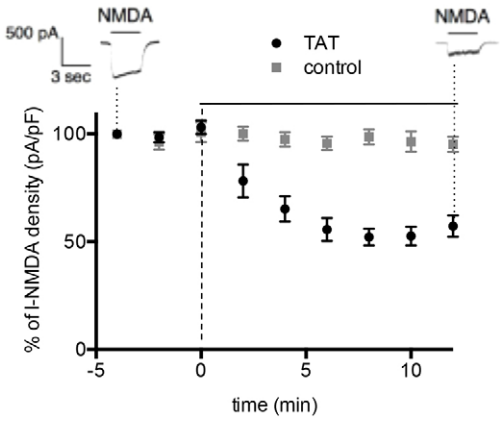

Fig. 5. Functional consequences of TAT dominant-negative peptides in disrupting the GKAP–DLC2 interaction. Endogenous NMDA currents (I-NMDA) were recorded in hippocampal neurons in the whole-cell patch-clamp configuration, before and during the perfusion of either dominant-negative peptides that inhibit the DLC2–GKAP interaction (TAT, black circles) or mutated peptides as a control (gray squares). Current density (pA/pF) over time was expressed as a percentage of the first NMDA application, with each point corresponding to one NMDA stimulation. The data show the mean±s.e.m. of current density recorded over time in seven neurons for each condition. Raw current traces are shown for the TAT condition 5 min before and 12 min after TAT perfusion.

DISCUSSION

Quantitative characterization of protein interactions in live cells remains one of the most important challenges in modern biology, as most key signaling events involve the modulation of protein complexes. In the present work, we investigated the molecular mechanisms by which DLC2 organizes GKAP-associated scaffolding complexes at the post-synapse and controls glutamate receptor function in synaptic transmission. The combination of the different experimental approaches used here (co-immunoprecipitation, cross-linking, BRET, structural modeling and sN&B experiments) provide strong consistent evidence that DLC2 must be homodimeric to bind to GKAP and that this interaction of DLC2 with GKAP promotes GKAP self-association, which is particularly apparent in neuronal spines. Finally, the integrity of the complex is required to potentiate glutamate receptor activity.

High-order complexes between Homer and Shank, the most abundant scaffolding proteins in the post-synaptic density (PSD), serve as a structural framework and assembly platform for other PSD proteins (Hayashi et al., 2009; Sheng and Hoogenraad, 2007). Among those PSD proteins, GKAP acts as an interface between Shank and PSD-95. Our results highlight the fact that GKAP also self-associates. In dendrites, GKAP homo-interactions are concentrated in spines and are further potentiated by the interaction with DLC2, increasing the level of complexity within the organization of the scaffolding complex at synapses. From sN&B experiments, we were able to calculate the number of particles contained within the average volume of a spine, and we found ~159.0±5.1 (±s.e.m.) particles containing DLC2 (with a mean stoichiometry of 16 DLC2 molecules per particle) and 66.1±2.2 particles containing GKAP (with a mean stoichiometry of 13 GKAP molecules per particle). Given that the range of endogenous expression levels was calculated to be ~150 GKAP proteins per PSD (Cheng et al., 2006) and knowing that the PSD comprises ~10% of the membrane surface area of the neuronal spine, these numbers attest the lack of overexpression, validating the biological relevance of studying the organization of transfected tagged proteins. The local concentration of GKAP and DLC2 in neuronal shafts and spines is clearly tightly regulated. Three distinct subcellular compartments containing DLC2 and GKAP were apparent from the sN&B experiments: (1) Intracellular pools containing a high concentration of GKAP and DLC2 proteins, mostly associated as homo-oligomers. The nature of this compartment will be defined by further investigation, but could serve as a stock container to allow protein turnover; (2) The dendritic shaft, which contains low levels of these proteins, associated as small oligomers composed mainly of 2 DLC2 and 2 GKAP proteins; (3) Dendritic spines, which display mostly heterologous complexes with oligomers of apparent average stoichiometries of 16 and 13 for DLC2 and GKAP, respectively, with higher-order oligomers correlated with a higher degree of heterologous interactions.

More insight into the biological role of DLC2 homodimerization was obtained using a mutant of DLC2 (in which Ser88 was mutated

to Glu to mimic constitutive phosphorylation), which was previously shown to display enhanced dissociation into monomers (Radnai et al., 2010). Unlike wild-type dimeric DLC2, this monomeric mutant showed no interaction with GKAP. These data are in agreement with crystal structures of DLC complexes, which show that bound partner peptides lie in two identical grooves formed at the dimerization interface (Liang et al., 1999; Tochio et al., 1998; Williams et al., 2007). Our present results are in line with previous hypotheses suggesting that one of the major roles of DLC dimers could be to promote the dimerization and stabilization of their interaction partners to form higher-order structures (Barbar, 2008; Wang et al., 2004). Although it is clear that GKAP self-association is favored by the binding of DLC2 dimer, the stability of heteromeric complexes might be rather weak. In cross-linking experiments (Fig. 2B,C) we confirmed that dimeric DLC2 efficiently increased the self-association of GKAP; however, the absence of staining at the expected molecular weight for 2DLC2–2GKAP complexes (300 kDa) suggests that this interaction is transitory. The results from sN&B show that the hetero-oligomers are confined predominantly to dendritic spines (Fig. 4). Localization of the oligomers to the spines means that they are located precisely where scaffold dynamics intervene in signal processing by controlling the function of synaptic receptors. By shifting the oligomerization equilibrium strongly towards the monomeric state and thus eliminating the binding grooves, phosphorylation of Ser88 of DLC2 could be an on/off switch in the remodeling of scaffolding complexes at the post-synapse. How these interactions of DLC2 as a hub protein are regulated remains to be revealed, but p21-activated protein kinase 1 (Pak1) or CaMK would be potential candidates. The active form of Pak1, phosphorylated Pak1, accumulates in punctae that colocalize with GKAP and PSD-95 (Zhang et al., 2005) and has been shown to phosphorylate DLC (Vadlamudi et al., 2004; Yang et al., 2005). In addition, a recent study revealed a role for CaMKII in the control of GKAP turnover at synapses (Shin et al., 2012).

Using a competitive TAT peptide to disrupt DLC2–GKAP complexes and, consequently, GKAP–GKAP and DLC2–DLC2 interactions, we quantified the stoichiometry of proteins in the complex, depending on subcellular compartments. It is important to note that these quantifications are based on the measurement of the minimal brightness for mCherry–DLC2 and Cerulean–GKAP found in the shaft in presence of the competitive peptide, which we calculated to be monomers. For example, the minimal brightness of wild-type mCherry–DLC2 in presence of the TAT peptide was similar to the brightness of the mCherry monomer in a control construct and also similar to the brightness of the 'monomeric' mutant of DLC2, mCherry–DLC2-S88E. According to these controls, we assumed that mCherry–DLC2 is a monomer in the shaft in presence of TAT. However, because the DLC2 homodimer forms a composite peptide-binding site, the TAT peptide should bind to a DCL2 dimer. Our results thus suggest that TAT binding to DLC2 dimer would be transient, as previously discussed for DLC2–GKAP interactions. The release of TAT would lead to an increase in the DCL2 monomer population. The molecular events leading to the transient binding are still to be investigated. By contrast, the tagged-DCL2 and the oligomeric state derived from these measurements are indicative of a lower limit and might underestimate the complex stoichiometry, given that dark wild-type DCL2 might be present. However, in neurons, proteins are confined in a restricted and limited space that would not allow the overexpression of proteins. It has been clearly shown indeed that recombinant protein displaces endogenous protein in a dose-dependent manner, indicating that the synaptic clustering of proteins is tightly regulated in neurons (see, for example, Specht et al., 2013). This notion of highly controlled regulation of constant protein expression is further supported by our present work. One powerful opportunity offered by sN&B is the ability to precisely quantify the number of recombinant proteins, which we found to be indeed in the range of usual endogenous protein expression level. Thus, even though we cannot exclude the presence of a weak endogenous protein expression, which would lead to an underestimate of the quantification of protein stoichiometry, our data suggest that recombinant proteins have replaced the endogenous ones.

Widely distributed in cytoplasm, DLC interacts with a variety of proteins (Barbar, 2008). Our current results provide further support for the notion of a hub protein stabilizing the helical structure of partially disordered proteins. Disruption of GKAP–DLC2 interactions in neuronal spines abolished the GKAP–GKAP association. Furthermore, after GKAP–DLC2 disruption, the DLC2–DLC2 interaction was re-localized to the membrane, probably through interaction with submembranous components of the actin-based membrane skeleton, emphasizing a reciprocal stabilization of the DLC2 homodimer by the interacting partners, as previously suggested for the DLC1–syntaphilin interaction (Chen et al., 2009). In their physiological environment, proteins rarely act in isolation but rather bind to other molecules to elicit specific subcellular responses. Associations to form dimers or higher-order oligomers confer several different structural and functional advantages to proteins, including improved stability, control over the accessibility or specificity of active sites and increased complexity. Consequent to the disruption of the GKAP–DLC2 hetero-oligomers, the preferential localization of GKAP to the spines was reduced and NMDA receptor activity decreased. This is in agreement with previous work showing that zGKAP overexpression enhances NMDA currents, whereas GKAPmut, which cannot interact with DLC2, does not (Moutin et al., 2012a). Hence, GKAP–DLC2 interactions play an important role in the modulation of NMDA neurotransmission. This oligomerization of scaffolding proteins represents a valuable means to control the clustering and function of receptor complexes and thereby to modulate synaptic transmission.

The application of two-photon two-color sN&B analysis has allowed spatially resolved quantification of the stoichiometry of a key heterologous protein complex implicated in the regulation of neuronal function. Two-photon excitation limits background fluorescence and provides a very small excitation volume, allowing reliable quantification, even in small structures, such as dendritic spines. Competitor-mediated dissociation of the complexes and spatial redistribution of the dissociated species were observed. Beyond the lessons learned about this specific system, the present results highlight the power of two-photon sN&B in quantitative systematic investigations of protein-interaction networks.

MATERIALS AND METHODS

Plasmids and TAT peptides

The p-Venus-DLC2, pmCherry-DLC2, pCerulean-GKAP1a, pRLuc8-GKAP1a, pCerulean-GKAP1a-mutant and pRLuc8-GKAP1a-mutant were as described previously (Moutin et al., 2012a). The coding sequence of Cerulean in pCerulean-GKAP1a and p-Venus were exchanged by molecular subcloning to obtain p-Venus-GKAP1a. From p-Venus-DLC2, we constructed p-Venus-DLC2-S88A by using a primer

containing point mutations; 5′-TTGCAATCCTCCTCTTCAAGGCCGGC-TAGGACCCA-3′. From p-Venus-DLC2-S88A, we constructed p-Venus-DLC2-S88E by using a primer containing point mutations; 5′-CAATCCTCCTCTTCAAGGAAGGCTAGGACC-3′. The plasmids pmCherry-DLC2-S88E and pmCherry-DLC2-S88A were obtained by molecular subcloning between p-Venus-DLC2-S88E, p-Venus-DLC2-S88A and p-mCherry-DLC2. pcDNA3-syntaxin-mCherry was obtained from the MGC (Montpellier Genomic Collection, France). TAT peptides were synthesized by Millegen, with a purity of >95%. The sequence of the TAT-GKAP-GIQVD peptide was YGRKKRRQRRRRCLSIGIQVDDAEES, and that of the TAT-GKAP-GVQVEE peptide was YGRKKRRQRRRKFQ-SVGVQVEEEKCFR. Both peptides were used together at 100 nM. Alternatively, we used the following mutated sequences as control peptides; GKAP-GNEND, YGRKKRRQRRRRCLSIGNENDDAEES and GKAP-GNENEE, YGRKKRRQRRRKFQSVGNENEEEKCFR.

Cell culture and transfection

HEK293 cell culture and transfection were performed as described previously (Perroy et al., 2004). Hippocampal neuronal primary cultures and transfection were performed as described previously (Moutin et al., 2012b). Briefly, primary cultures were prepared from embryonic day 17.5 mice, transfected at days *in vitro* (DIV)10 or 11 using Lipofectamine 2000 (Invitrogen, Cergy Pontoise, France) and studied between DIV11 and DIV14.

BRET measurements

BRET measurements in cell population using a spectrophotometric plate reader were performed as described previously (Perroy et al., 2008).

Cross-linking

Transfected HEK cells were washed twice in ice-cold PBS containing 1 mM $CaCl_2$ and 0.5 mM $MgCl_2$ (PBS-CM). GKAP and DLC2 oligomers were cross-linked using 2 mM NHS-LC-diazirine (SDA) crosslinkers (Pierce) for 30 min at 4℃ in PBS-CM. After quenching with 20 mM Tris-HCl pH 8.8, UV irradiation (using a 365-nm UV bulb) was performed for 15 min before cells were scraped in lysis buffer [20 mM HEPES pH 7.4, 100 mM NaCl, 5 mM EDTA, 1% NP40, supplemented with the Halt Protease and phosphatase inhibitor cocktail (Pierce)]. After 30 min of solubilisation at 4℃, lysates were centrifuged (16,000 ***g***, 10 min, 4℃). Supernatant was collected and mixed with LDS sample buffer (Invitrogen) supplemented with 10% β-mercaptoethanol and incubated at 80℃ for 5 min. Proteins were separated on 4–12% Bis-Tris gels (NuPage Novex, Invitrogen) and transferred to nitrocellulose membranes. Proteins were detected using anti-GFP (1:1000, Roche, recognizes Venus) or anti-RFP (1:1000, MBL, recognizes mCherry) antibodies and HRP-coupled secondary antibodies. Quantification of band intensity was performed using the Molecular Imaging Software (Carestream).

Immunoprecipitation

Cells were lysed in 0.1% Triton X-100, 150 mM NaCl, 2 mM EGTA, anti-protease mixture (Roche Applied Science), 2 mM DTT and 20 mM Tris-HCl pH 7.4 (lysis buffer) and centrifuged. The lysate obtained from 10^7 transfected cells was mixed with RFP–Trap-A (ChromoTek, recognizes mCherry) and incubated for 1 h at room temperature. After washing, the solid phase was incubated in Laemmli buffer at 60℃. Protein samples were resolved by PAGE on a 7.5% gel, transferred to nitrocellulose and subjected to immunoblotting using rabbit anti-GFP antibody (1:1000, Invitrogen, recognizes Venus and Cerulean) or anti-RFP antibody (1:1000, MBL, recognizes mCherry) for 1 h. The blots were then washed three times with PBS containing 0.1% Tween-20 (PBST). The nitrocellulose was then incubated with DyLight™-800-conjugated goat anti-rabbit-IgG (H^+L) (Pierce) for 1 h. The blots were then washed three times with PBST. Proteins were visualized by scanning on an Odyssey Infrared Imaging System (LI-COR Biosciences) using the 800-nm channel. The total level of proteins was determined to evaluate equal transfection efficiency. Quantification was performed, and the values were expressed as a percentage of the ratio of co-immunoprecipitated Venus-tagged proteins to immunoprecipitated mCherry-tagged proteins.

Electrophysiological recordings and data analysis

Electrophysiological recordings were performed as described previously (Moutin et al., 2012a). Whole-cell NMDA currents (I-NMDA) were evoked in neurons by a short (3 s) application of 100 µM NMDA (Sigma-Aldrich, St Quentin Fallavier, France) every 2 min. We measured the peak I-NMDA amplitude. After 5 min of I-NMDA control recording, TAT-peptides (GIQVD+GVQVEE, 100 nM each, diluted in medium) were perfused until the end of the recording. All electrophysiological data were analyzed using the Clampfit 10 software from Axon Instruments (Molecular Devices).

Fluorescence fluctuation microscopy – sN&B in two-photon mode

Two-photon scanning cross number and brightness extends fluorescence cross-correlation spectroscopy (FCCS, Savatier et al., 2010) to two-dimensional cellular images by a covariance analysis of the raster-scanned fluorescence fluctuations in two channels. Scanning-mode two-photon approaches have proven to be particularly powerful in this respect (Digman et al., 2008; Digman et al., 2009). Cross number and brightness uses the variance in the fluorescence intensity at each pixel of a stack of rapid raster scans to calculate the number (N) of fluorescent molecules, as well as their molecular brightness (B), which reflects the degree of homo-oligomerization (in counts per pixel dwell-time per molecule). In two-color mode (using Cerulean and mCherry fluorescent protein fusions for each of two interacting protein partners, for example), calculation of the covariance between the intensity fluctuations in the blue and red detection channels allows evaluation of the cross-brightness (Bcc) or co-variance of the intensities (Digman et al., 2009). Non-zero Bcc is only observed in the case of co-diffusion of the fluorescent molecules present in the sample at the observed pixels, and hence is an absolute quantitative measure of protein hetero-complex formation. Because shot noise between detectors does not co-vary, the Bcc is a particularly sensitive and reliable indicator of heterologous protein interactions. Cross number and brightness uses two species that are independently labeled with two spectrally separated fluorescent probes (mCherry–DLC2 and Cerulean–GKAP). These fluorescent probes are excited by two-photon excitation simultaneously using a single femtosecond pulsed infrared laser tuned to 950 nm (Tsunami, Newport, DE). Their fluorescence is detected on two separate avalanche photodiode detectors with appropriate dichroics and filters to separate the blue and red emission [ISS, Champaign, IL; dichroic filter 505DCXR (chroma, AHF analysentechnik, Tuebingen, Germany). Bandpass filter for channel 1, 653/95 (chroma, AHF analysentechnik, Tuebingen, Germany) and bandpass filter for channel 2, 455/100 (chroma, AHF analysentechnik, Tuebingen, Germany)]. After filtering out the infrared exciting light using a 720 shortpass infrared blocking filter, the fluorescence emission light was split into two channels using a dichroic filter (505DCXR) and a bandpass filter for channel 1 (653/95) and for channel 2 (455/100), all from Chroma (Tuebingen, Germany). The excitation volume was calibrated as diffraction-limited two-photon PSF using 60 nM Rhodamine with a ω_o value of 400 nm and a z_o value of 1.4 µm.

The variance at each pixel in a series of raster scans allows for decomposition of the fluorescence signal into the number of fluorescent particles and their molecular brightness, and the cross-variance (Bcc) between two channels allows an estimation of the degree of complex formation:

$$N(\text{molecules}) \times B(\text{counts/s/molecule}) = F(\text{counts/s}),$$

where

$$B = \frac{\sigma^2}{<F>} \text{ and } N = \frac{<F>^2}{\sigma^2}.$$

Brightness values were corrected for the contribution of shot noise by subtracting 1 to yield the true brightness, ε;

$$\varepsilon = B - 1,$$

and the true number of molecules, n, was then calculated using the formula

$$n = \frac{(N \times B)}{\varepsilon}$$

(Digman et al., 2008). The cross brightness, Bcc, is calculated as the normalized covariance of the intensity fluctuations between the two channels;

$$Bcc = \frac{\sigma_{Ch1} \times \sigma_{Ch2}}{<F>_{Ch1} \times <F>_{Ch2}}.$$

The Bcc is a true value because detector shot noise is uncorrelated, and it is equivalent to the G_{ox} value in fluorescence cross-correlation analysis. The data were analyzed using the SimFCS software (LFD, Irvine, CA).

Sequence-structure analysis

Secondary structure prediction and local sequence conservation were analyzed using the server Jpred3 (Cole et al., 2008). Analysis of the DLC2 peptide interactions were performed at the atomic level using the available crystal structures at high resolution [Protein Data Bank (PDB) ID 2XQQ, see Rapali et al., 2011; and PDB ID 1CMI, see Liang et al., 1999] and the software Coot (Emsley and Cowtan, 2004). In parallel, models of the 2:1 and 2:2 complexes were built using MODELLER (Šali and Blundell, 1993) to show that the close contacts in the 2:1 model do not fit with the sequence variation observed among close homologs and that the predicted disordered structure favors the 2:2 model (see text).

Acknowledgements

We would like to thank Enrico Gratton (University of California, Irvine, CA) for helpful discussions and for custom modification of the SimFCS analysis software. We thank Sabine Lévi (Institut du Fer Á Moulin, Paris, France) for relevant remarks. We thank the Platform of Pharmacology at the Institute of Functional Genomics.

Competing interests

The authors declare no competing interests.

Author contributions

J.P. conceived research; E.M., C.R. and J.P. designed research; E.M., V.C., F.R., C.C., N.B., M.F. and J.P. performed research; E.M., V.C., C.C., L.F., C.R. and J.P. analyzed the data; G.L. performed the sequence-structure analysis; C.R. and J.P. wrote the paper and all authors reviewed the paper.

Funding

We acknowledge support from the French Infrastructure for Integrated Structural Biology (FRISBI) [grant number ANR-10-INSB-05-01]. This work was supported by the European Community [grant number Health-F2-2008-222918, REPLACES]; Agence Nationale de la Recherche [grant numbers ANR-11-BSV4-018-03, DELTAPLAN and ANR-13-JSV4-0005-01]; Fondation Jérôme Lejeune; the Fonds Unique Interministériel RHENEPI and DIATRAL; and the Région Languedoc-Roussillon (Chercheur d'Avenir). Part of this work was performed in the frame of the Proof of Concept Studies for the European Strategy Forum on Research Infrastructures project Euro-BioImaging at the PCS facility number 38.

References

Barbar, E. (2008). Dynein light chain LC8 is a dimerization hub essential in diverse protein networks. *Biochemistry* **47**, 503-508.

Benashski, S. E., Harrison, A., Patel-King, R. S. and King, S. M. (1997). Dimerization of the highly conserved light chain shared by dynein and myosin V. *J. Biol. Chem.* **272**, 20929-20935.

Benison, G., Nyarko, A. and Barbar, E. (2006). Heteronuclear NMR identifies a nascent helix in intrinsically disordered dynein intermediate chain: implications for folding and dimerization. *J. Mol. Biol.* **362**, 1082-1093.

Benison, G., Chiodo, M., Karplus, P. A. and Barbar, E. (2009). Structural, thermodynamic, and kinetic effects of a phosphomimetic mutation in dynein light chain LC8. *Biochemistry* **48**, 11381-11389.

Bockaert, J., Perroy, J., Bécamel, C., Marin, P. and Fagni, L. (2010). GPCR interacting proteins (GIPs) in the nervous system: Roles in physiology and pathologies. *Annu. Rev. Pharmacol. Toxicol.* **50**, 89-109.

Chen, Y. M., Gerwin, C. and Sheng, Z. H. (2009). Dynein light chain LC8 regulates syntaphilin-mediated mitochondrial docking in axons. *J. Neurosci.* **29**, 9429-9438.

Cheng, D., Hoogenraad, C. C., Rush, J., Ramm, E., Schlager, M. A., Duong, D. M., Xu, P., Wijayawardana, S. R., Hanfelt, J., Nakagawa, T. et al. (2006). Relative and absolute quantification of postsynaptic density proteome isolated from rat forebrain and cerebellum. *Mol. Cell. Proteomics* **5**, 1158-1170.

Cole, C., Barber, J. D. and Barton, G. J. (2008). The Jpred 3 secondary structure prediction server. *Nucleic Acids Res.* **36**, W197-W201.

Dietz, G. P. and Bähr, M. (2005). Peptide-enhanced cellular internalization of proteins in neuroscience. *Brain Res. Bull.* **68**, 103-114.

Digman, M. A., Dalal, R., Horwitz, A. F. and Gratton, E. (2008). Mapping the number of molecules and brightness in the laser scanning microscope. *Biophys. J.* **94**, 2320-2332.

Digman, M. A., Wiseman, P. W., Choi, C., Horwitz, A. R. and Gratton, E. (2009). Stoichiometry of molecular complexes at adhesions in living cells. *Proc. Natl. Acad. Sci. USA* **106**, 2170-2175.

Emsley, P. and Cowtan, K. (2004). Coot: model-building tools for molecular graphics. *Acta Crystallogr. D* **60**, 2126-2132.

Fejtova, A., Davydova, D., Bischof, F., Lazarevic, V., Altrock, W. D., Romorini, S., Schöne, C., Zuschratter, W., Kreutz, M. R., Garner, C. C. et al. (2009). Dynein light chain regulates axonal trafficking and synaptic levels of Bassoon. *J. Cell Biol.* **185**, 341-355.

Fuhrmann, J. C., Kins, S., Rostaing, P., El Far, O., Kirsch, J., Sheng, M., Triller, A., Betz, H. and Kneussel, M. (2002). Gephyrin interacts with Dynein light chains 1 and 2, components of motor protein complexes. *J. Neurosci.* **22**, 5393-5402.

Hayashi, M. K., Tang, C., Verpelli, C., Narayanan, R., Stearns, M. H., Xu, R. M., Li, H., Sala, C. and Hayashi, Y. (2009). The postsynaptic density proteins Homer and Shank form a polymeric network structure. *Cell* **137**, 159-171.

Jaffrey, S. R. and Snyder, S. H. (1996). PIN: an associated protein inhibitor of neuronal nitric oxide synthase. *Science* **274**, 774-777.

Lee, K. H., Lee, S., Kim, B., Chang, S., Kim, S. W., Paick, J. S. and Rhee, K. (2006). Dazl can bind to dynein motor complex and may play a role in transport of specific mRNAs. *EMBO J.* **25**, 4263-4270.

Liang, J., Jaffrey, S. R., Guo, W., Snyder, S. H. and Clardy, J. (1999). Structure of the PIN/LC8 dimer with a bound peptide. *Nat. Struct. Biol.* **6**, 735-740.

Lo, K. W., Kan, H. M., Chan, L. N., Xu, W. G., Wang, K. P., Wu, Z., Sheng, M. and Zhang, M. (2005). The 8-kDa dynein light chain binds to p53-binding protein 1 and mediates DNA damage-induced p53 nuclear accumulation. *J. Biol. Chem.* **280**, 8172-8179.

Makokha, M., Huang, Y. J., Montelione, G., Edison, A. S. and Barbar, E. (2004). The solution structure of the pH-induced monomer of dynein light-chain LC8 from Drosophila. *Protein Sci.* **13**, 727-734.

Mercier, J. F., Salahpour, A., Angers, S., Breit, A. and Bouvier, M. (2002). Quantitative assessment of beta 1- and beta 2-adrenergic receptor homo- and heterodimerization by bioluminescence resonance energy transfer. *J. Biol. Chem.* **277**, 44925-44931.

Moutin, E., Raynaud, F., Fagni, L. and Perroy, J. (2012a). GKAP-DLC2 interaction organizes the postsynaptic scaffold complex to enhance synaptic NMDA receptor activity. *J. Cell Sci.* **125**, 2030-2040.

Moutin, E., Raynaud, F., Roger, J., Pellegrino, E., Homburger, V., Bertaso, F., Ollendorff, V., Bockaert, J., Fagni, L. and Perroy, J. (2012b). Dynamic remodeling of scaffold interactions in dendritic spines controls synaptic excitability. *J. Cell Biol.* **198**, 251-263.

Naisbitt, S., Kim, E., Tu, J. C., Xiao, B., Sala, C., Valtschanoff, J., Weinberg, R. J., Worley, P. F. and Sheng, M. (1999). Shank, a novel family of postsynaptic density proteins that binds to the NMDA receptor/PSD-95/GKAP complex and cortactin. *Neuron* **23**, 569-582.

Naisbitt, S., Valtschanoff, J., Allison, D. W., Sala, C., Kim, E., Craig, A. M., Weinberg, R. J. and Sheng, M. (2000). Interaction of the postsynaptic density-95/guanylate kinase domain-associated protein complex with a light chain of myosin-V and dynein. *J. Neurosci.* **20**, 4524-4534.

Navarro, C., Puthalakath, H., Adams, J. M., Strasser, A. and Lehmann, R. (2004). Egalitarian binds dynein light chain to establish oocyte polarity and maintain oocyte fate. *Nat. Cell Biol.* **6**, 427-435.

Nyarko, A., Hare, M., Hays, T. S. and Barbar, E. (2004). The intermediate chain of cytoplasmic dynein is partially disordered and gains structure upon binding to light-chain LC8. *Biochemistry* **43**, 15595-15603.

Perroy, J., Pontier, S., Charest, P. G., Aubry, M. and Bouvier, M. (2004). Real-time monitoring of ubiquitination in living cells by BRET. *Nat. Methods* **1**, 203-208.

Perroy, J., Raynaud, F., Homburger, V., Rousset, M. C., Telley, L., Bockaert, J. and Fagni, L. (2008). Direct interaction enables cross-talk between ionotropic and group I metabotropic glutamate receptors. *J. Biol. Chem.* **283**, 6799-6805.

Puthalakath, H., Huang, D. C., O'Reilly, L. A., King, S. M. and Strasser, A. (1999). The proapoptotic activity of the Bcl-2 family member Bim is regulated by interaction with the dynein motor complex. *Mol. Cell* **3**, 287-296.

Radnai, L., Rapali, P., Hódi, Z., Süveges, D., Molnár, T., Kiss, B., Bécsi, B., Erdödi, F., Buday, L., Kardos, J. et al. (2010). Affinity, avidity, and kinetics of target sequence binding to LC8 dynein light chain isoforms. *J. Biol. Chem.* **285**, 38649-38657.

Rapali, P., Radnai, L., Süveges, D., Harmat, V., Tölgyesi, F., Wahlgren, W. Y., Katona, G., Nyitray, L. and Pál, G. (2011). Directed evolution reveals the

binding motif preference of the LC8/DYNLL hub protein and predicts large numbers of novel binders in the human proteome. *PLoS ONE* **6**, e18818.

Raux, H., Flamand, A. and Blondel, D. (2000). Interaction of the rabies virus P protein with the LC8 dynein light chain. *J. Virol.* **74**, 10212-10216.

Renner, M., Specht, C. G. and Triller, A. (2008). Molecular dynamics of postsynaptic receptors and scaffold proteins. *Curr. Opin. Neurobiol.* **18**, 532-540.

Šali, A. and Blundell, T. L. (1993). Comparative protein modelling by satisfaction of spatial restraints. *J. Mol. Biol.* **234**, 779-815.

Savatier, J., Jalaguier, S., Ferguson, M. L., Cavaillès, V. and Royer, C. A. (2010). Estrogen receptor interactions and dynamics monitored in live cells by fluorescence cross-correlation spectroscopy. *Biochemistry* **49**, 772-781.

Scannevin, R. H. and Huganir, R. L. (2000). Postsynaptic organization and regulation of excitatory synapses. *Nat. Rev. Neurosci.* **1**, 133-141.

Schnorrer, F., Bohmann, K. and Nüsslein-Volhard, C. (2000). The molecular motor dynein is involved in targeting swallow and bicoid RNA to the anterior pole of Drosophila oocytes. *Nat. Cell Biol.* **2**, 185-190.

Sheng, M. and Hoogenraad, C. C. (2007). The postsynaptic architecture of excitatory synapses: a more quantitative view. *Annu. Rev. Biochem.* **76**, 823-847.

Shin, S. M., Zhang, N., Hansen, J., Gerges, N. Z., Pak, D. T., Sheng, M. and Lee, S. H. (2012). GKAP orchestrates activity-dependent postsynaptic protein remodeling and homeostatic scaling. *Nat. Neurosci.* **15**, 1655-1666.

Song, Y., Benison, G., Nyarko, A., Hays, T. S. and Barbar, E. (2007). Potential role for phosphorylation in differential regulation of the assembly of dynein light chains. *J. Biol. Chem.* **282**, 17272-17279.

Song, C., Wen, W., Rayala, S. K., Chen, M., Ma, J., Zhang, M. and Kumar, R. (2008). Serine 88 phosphorylation of the 8-kDa dynein light chain 1 is a molecular switch for its dimerization status and functions. *J. Biol. Chem.* **283**, 4004-4013.

Specht, C. G., Izeddin, I., Rodriguez, P. C., El Beheiry, M., Rostaing, P., Darzacq, X., Dahan, M. and Triller, A. (2013). Quantitative nanoscopy of inhibitory synapses: counting gephyrin molecules and receptor binding sites. *Neuron* **79**, 308-321.

Tochio, H., Ohki, S., Zhang, Q., Li, M. and Zhang, M. (1998). Solution structure of a protein inhibitor of neuronal nitric oxide synthase. *Nat. Struct. Biol.* **5**, 965-969.

Tu, J. C., Xiao, B., Naisbitt, S., Yuan, J. P., Petralia, R. S., Brakeman, P., Doan, A., Aakalu, V. K., Lanahan, A. A., Sheng, M. et al. (1999). Coupling of mGluR/Homer and PSD-95 complexes by the Shank family of postsynaptic density proteins. *Neuron* **23**, 583-592.

Vadlamudi, R. K., Bagheri-Yarmand, R., Yang, Z., Balasenthil, S., Nguyen, D., Sahin, A. A., den Hollander, P. and Kumar, R. (2004). Dynein light chain 1, a p21-activated kinase 1-interacting substrate, promotes cancerous phenotypes. *Cancer Cell* **5**, 575-585.

Wang, W., Lo, K. W., Kan, H. M., Fan, J. S. and Zhang, M. (2003). Structure of the monomeric 8-kDa dynein light chain and mechanism of the domain-swapped dimer assembly. *J. Biol. Chem.* **278**, 41491-41499.

Wang, L., Hare, M., Hays, T. S. and Barbar, E. (2004). Dynein light chain LC8 promotes assembly of the coiled-coil domain of swallow protein. *Biochemistry* **43**, 4611-4620.

Williams, J. C., Roulhac, P. L., Roy, A. G., Vallee, R. B., Fitzgerald, M. C. and Hendrickson, W. A. (2007). Structural and thermodynamic characterization of a cytoplasmic dynein light chain-intermediate chain complex. *Proc. Natl. Acad. Sci. USA* **104**, 10028-10033.

Xiao, F., Weng, J., Fan, K. and Wang, W. (2010). Mechanism of Ser88 phosphorylation-induced dimer dissociation in dynein light chain LC8. *J. Phys. Chem. B* **114**, 15663-15672.

Yang, Z., Vadlamudi, R. K. and Kumar, R. (2005). Dynein light chain 1 phosphorylation controls macropinocytosis. *J. Biol. Chem.* **280**, 654-659.

Zeke, A., Lukács, M., Lim, W. A. and Reményi, A. (2009). Scaffolds: interaction platforms for cellular signalling circuits. *Trends Cell Biol.* **19**, 364-374.

Zhang, H., Webb, D. J., Asmussen, H., Niu, S. and Horwitz, A. F. (2005). A GIT1/PIX/Rac/PAK signaling module regulates spine morphogenesis and synapse formation through MLC. *J. Neurosci.* **25**, 3379-3388.